

# Double Refraction Modeling for Accurate Visibility Trees in the Method of Images

ROMAN NOVAK

Department of Communication Systems

Jožef Stefan Institute

Jamova 39, 1000 Ljubljana

SLOVENIA

roman.novak@ijs.si

*Abstract:* Method of images (MI) is one of the oldest methods for radio wave propagation prediction based on the ray-tracing principle. Although the MI was originally restricted to the radio environments with prevailing reflection phenomena, it is also used in indoor scenarios in which through-wall transmission make a significant contribution to the received signal power. Exact handling of propagation paths, either in the form of polyhedra bounding regions or in the form of some other equivalent geometrical description, is usually complemented with the use of visibility trees to contain excessive growth of source images. However, strict visibility trees and double refractions on parallel planes involved in through-wall transmissions are not well-suited to each other. Here we study visibility inaccuracy, which is usually ignored. We propose a source image translation heuristic based on the wall depth, material and field of view. We show that the proposed double refraction modeling improves accuracy of strict visibility trees, which gives a better fit of predicted signal to the theoretically correct solution.

*Key-Words:* Ray tracing, Radio propagation prediction, Method of images, Double refraction

## 1 Introduction

The prediction of electromagnetic wave propagation is at the core of any wireless system design and essential for many services. When accompanied with detailed knowledge of the environment geometry, advanced ray-tracing techniques take into account the majority of paths the real wavefront would traverse and model actual physical phenomena responsible for propagation of electromagnetic waves. Advanced channel characteristics, including delay spread and direction of arrival can be calculated from multipath traces, which are not readily available in pure stochastic propagation predictions.

Two computationally distinct ray-tracing approaches have been followed since early beginnings. The SBR (shooting and bouncing rays) is often seen as the brute force approach, effectively tracing a large number of rays from the transmitting source in all directions into the scene. On the other hand, the MI (method of images) evaluates feasible propagation regions without resorting to a single ray granularity. The MI is characterized by excellent prediction accuracy while modeling reflections and through-wall transmissions, largely because it does not depend on the notion of reception spheres to detect rays contributing to a signal at a given point in space.

The MI is designed around the observation that

rays reflected from a surface seem to originate from a fictitious transmission source, which can be found symmetrically on the other side of the surface along its perpendicular. Such a fictitious source is called a source image. Multiple reflections are accounted for by considering existing images as new transmission points, which recursively leads to the image tree. Finite shapes of surfaces limit reflected regions to polyhedron volumes, which reduces the size of a tree description. If the image tree describes only viable propagation paths, then it is referred to as a visibility tree.

Visibility trees are not limited to reflected paths. Through-wall transmission caused by double refraction phenomena is commonly dealt with by extending the source mirroring onto walls that are identified in the so-called transmission regions [1]. However, modeling refraction is more challenging and some compromises must be made that affect the accuracy of visibility trees. At the core of the problem is the distortion of a spherical wavefront as it enters different medium of transmission. Rays that model the wavefront bend with respect to incident angle, ruining the polyhedron shapes of volumes in which these rays propagate after passing into different medium. Similar observation holds if visible surfaces are used instead of propagation volumes.

Consequently, proposals that incorporate trans-

mission branches in the visibility tree normally model objects as slabs with predefined thickness, such as walls, for which double refraction on the front and on the back surface to some extent cancels out the error. A straight line of the through-the-object rays is usually assumed for visibility resolution, which is a good approximation only for a thin slab located far from the source.

Here we propose a translation of the source image location in the direction opposite to the surface normal in order to increase the visibility tree accuracy while keeping the original source location for the second signal-backtracking step. Note that a backtracking is always required to re-create signal paths, even in a strict visibility tree, at least to establish the length of a path and all the reflection coefficients affecting the radio signal power. We show the improvement in the visibility tree accuracy for a heuristic based on the wall depth, material and field of view.

In the following, Section 2 reviews the related work. The distortion and the proposed correction of a double refraction on parallel planes are studied in Section 3. Section 4 quantifies the visibility error and its reduction. A short conclusion follows in Section 5.

## 2 Related Work

Method of images has been known since the first attempts to predict electromagnetic wave propagation for radio communications [2]. Ikegami et al. [3] were among the first who showed the usefulness of ray-tracing technique for radio wave propagation prediction in 1991, which was initially used in computer graphics domain. A larger set of electromagnetic effects are typically dealt with at radio frequencies. For example, diffraction [4] and interference are generally not considered in the global illumination problem, although some exceptions exist [5].

We have seen numerous refinements of the method of images in the past two decades. Soon after its introduction, proposals to reduce the over dimensioned image tree emerged. In the following, we restrict ourselves to the published works that support full 3D environment modeling through the entire computation and to the ones being most relevant to our proposal.

The elaborate method of regions [1] constrains physically feasible paths by introducing spatial regions in the shape of convex polyhedra into the image tree construction. Computing viable reflection or transmission regions translate to the polyhedra intersection problem, the solution of which involves intensive computational geometry. Simplified version of the spatial regions treatment can be found in [6],

where the geometry of objects is restricted to horizontal walls of arbitrary shape and strictly rectangular vertical walls.

Instead of bounding regions, [7] deals with a set of visible surfaces contained within such feasible regions. Surfaces are represented by polygons as seen from the source image after the surface corners have been projected to the viewing plane. In order to extract polygons describing only visible parts of a surface, each projection is processed by a sweep-line algorithm, followed by the well-known graph-theoretic polygon subtraction to account for hidden parts of a surface. The reflection visibility window is represented by yet another polygon in the computation, generally hindered by the treatment of many special cases.

Visibility tree in [8] is only partially reduced image tree because it is based on a polar-sweep of 2D space. When applied to 3D scene in the second backtracking step, paths described by the tree may or may not give rise to actual paths and further checks are still needed. Further, being a hybrid 2D/3D method, ground, floors and ceilings must be treated separately.

Computer graphics rendering of reflections and double refractions is proposed in [9] as an efficient way to construct strict visibility trees using task parallelization capabilities of the latest GPUs. Visible surfaces are identified in a graphical framebuffer using standard stencil, z-buffering and plane clipping.

Further attempts to reduce image tree size while keeping the support for full 3D computation involve various pre-processing steps on the input geometry, such as dividing surfaces into tiles and using the tile center as the ray interaction point [10], pre-computing intermediate values needed in the highly repetitive intersection tests, such as angular relations between the scene objects [11], or just taking advantage of parallel tasks to speed up the computation [12].

However, none of the above work has addressed the problem of inaccurate transmission regions, either modeling only reflections or assuming a straight line of the through-the-wall rays for the visibility region confinement.

## 3 Translation of a Double Refraction Source

Visibility tree consists of nodes each describing a single unobstructed segment of a viable ray path. Scene surfaces initially visible from the source and latter from its images dictate branching of the tree. Segments of viable ray paths are mathematically described either as polyhedron-shaped regions or as shapes of visible surfaces. However, the assumption

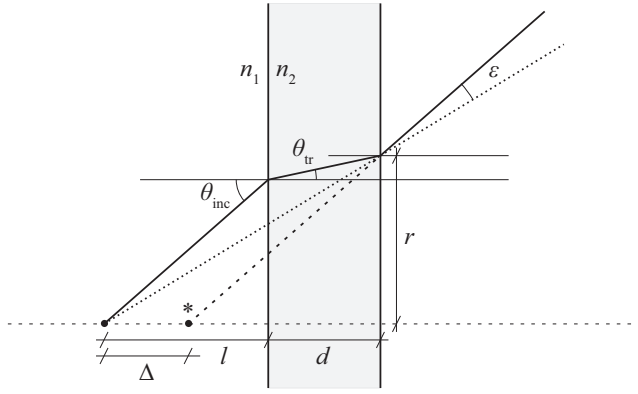


Fig. 1. Double refraction on parallel planes

of rays spreading in regions modelled as solids with flat polygonal faces is obviously false when it comes to refraction modeling. Due to Snell's law of refraction, a spherical wavefront takes a hyperbolic shape [13] after it passes through a plane interface into new propagation medium. An attempt to find a common source image for a single refraction by extending refracted rays back toward the origin would necessary fail. Situation improves considerably for double refractions on parallel planes. Rays re-entering the initial transmission medium realigns with the incident ray's direction on the second refraction. As illustrated in Fig. 1, a small parallel displacement still remains.

Shown displacement is commonly ignored. One of the reasons for not attempting to correct the through-wall transmission inaccuracy when building strict visibility trees is its dependence on the incident angle  $\theta_{inc}$ , which would make flat polygonal faces inappropriate for describing exact visibility regions. Nevertheless, as shown in the following, a translation of the source image in the direction opposite to the surface normal, i.e.,  $\Delta$  in Fig. 1, reduces the misalignment angle to a fraction of a degree and decreases the error even if we keep existing imperfect but geometrically favorable methods of describing regions.

First, we define the misalignment angle  $\varepsilon$  between the double-refracted ray and the matching line-of-sight direction from the  $\Delta$ -corrected source image as

$$\varepsilon = \theta_{inc} - \tan^{-1}(r/(l + d - \Delta)) \quad (1)$$

with

$$r = l \tan \theta_{inc} + d \tan \theta_{tr}, \quad (2)$$

where  $l$  is the source to wall distance,  $d$  is the depth of a wall,  $\theta_{inc}$  is the ray's angle of incidence and  $\theta_{tr}$  is the angle of transmission for media refractive indices  $n_1$  and  $n_2$  in compliance with  $\sin \theta_{tr} = (n_1/n_2) \sin \theta_{inc}$ .

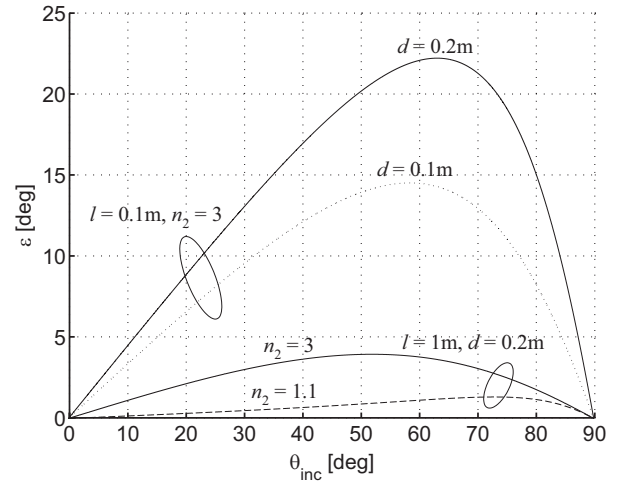


Fig. 2. Double refraction misalignment error versus angle of incidence

Note that  $\varepsilon$  shown in Fig. 1 is for untranslated source image.

In Fig. 2, we quantify  $\varepsilon$  versus the incident angle. The problem is most severe for source images close to the wall and diminishes with increasing wall distance. For example, having a transmission source in front of a 20 cm thick heavy-concrete wall with refractive index of 3 at 10 cm distance and 60-degree incident angle gives 22.1-degree misalignment between the double-refracted ray and the matching line-of-sight direction. The problem is significantly less severe for more distant sources, e.g., at 1 m the misalignment already reduces to 3.8 degrees with all other parameters unchanged. Next, thicker walls generally increase  $\varepsilon$  as shown by the upper two curves. As expected, lower index of refraction causes less ray bending and thus less visibility deviations, which is demonstrated by the lower two curves in Fig. 2. In all examples  $n_1$  equals 1.

### 3.1 Source Image Translation

Not knowing further signal interactions with scene geometry, correction  $\Delta$  would ideally be selected in a way to minimize the expected misalignment angle over the incident angles for the actually visible parts of the wall. Formally, one would have to find  $\Delta$  that minimizes

$$\Delta_{min} = \arg \min_{\Delta} \frac{1}{\Omega_0} \int_{\Omega_0} |\varepsilon| d\Omega, \quad (3)$$

where  $\Omega_0$  is the solid angle covered by the visible parts of the wall and  $d\Omega$  is the differential solid angle. The irregular shape of  $\Omega_0$  does not allow efficient algebraic treatment of (3). Further, numerical evaluation of (3) would be computationally prohibitive

in most ray-tracing applications and some simplifications must be made.

At the very least, the information about the wall's corners is always available, from which limits on the angle of incidence can be derived with minimal effort. Let  $[\theta_{\min}, \theta_{\max}]$  be the range of incident angles for a surface facing the source image, with  $0 \leq \theta_{\min} < \theta_{\max}$ . It is important to note that all incident angles should be accounted for when calculating  $\theta_{\min}$  and  $\theta_{\max}$ . While  $\theta_{\max}$  is actually maximal incident angle at one of the four front-facing corners, this is not true for minimal incident angle. If the closest point to the source image in the front-facing plane is within the wall edges, then  $\theta_{\min}$  is 0. Otherwise, incident angle of the closest point located on one of the wall's edges should be used to comply with the above range definition. We approximate  $\Delta_{\min}$  by requiring zero misalignment at

$$\theta^* = \frac{\theta_{\min} + \theta_{\max}}{2}. \quad (4)$$

Taking a simple average of the incident angle range is motivated by irregular wall shapes and sizes and their diverse relative positions to the source image. Better approximation is associated with increased computation times and minor accuracy improvements, as shown in the following section.

The source image translation is then calculated as

$$\Delta = \left(1 - \frac{\cos \theta^*}{\sqrt{(n_2/n_1)^2 - \sin^2 \theta^*}}\right)d. \quad (5)$$

Expression (5) is derived by setting  $\varepsilon$  to zero and replacing  $\theta_{\text{inc}}$  with  $\theta^*$  in (1). Substituting (2) for  $r$  further eliminates distance  $l$  from the equation. Using the relationship between the incident angle and the refracted angle in addition to some basic trigonometric identities leads to  $\Delta$  being dependent only on the refractive indices, wall's depth  $d$  and chosen  $\theta^*$ .

## 4 Evaluation

### 4.1 Misalignment Angle

First we study the reduction of misalignment angle by applying correction  $\Delta$  to the source image in the scenario of a 20 cm thick wall at 1 m distance, for which 4-degree maximum visibility error is shown in Fig. 2. If no information about the wall shape is known, one could use at least theoretically unlimited refraction planes, i.e.,  $\theta_{\min} = 0$  and  $\theta_{\max} = \pi/2$ , which gives 45-degree  $\theta^*$  and 15.2 cm correction  $\Delta$ . This results in under 0.5-degree misalignment, shown as dashed line in Fig. 3. For most of incident angles the error is even

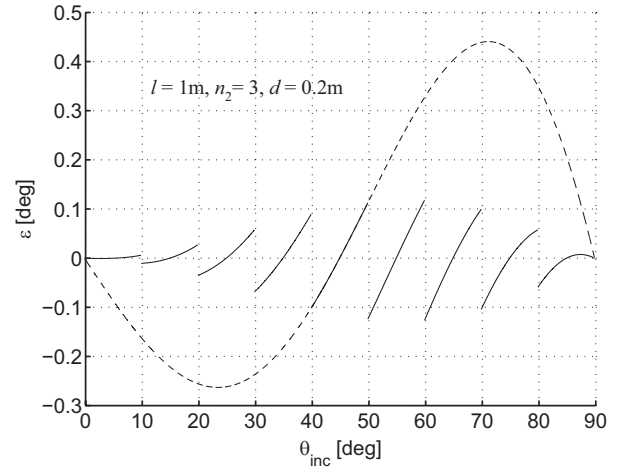


Fig. 3. Misalignment error in  $\Delta$ -corrected double refractions; walls with 10-degree field of view (solid lines) and a wall with theoretically unlimited refraction planes (dashed line) are considered.

smaller, demonstrating that the source image translation improves accuracy even if shape of the wall is not taken into account.

When the limits on the incident angles are available, source image correction can be fine-tuned to the field of view. For the above scenario with a fixed size wall that is visible at 10-degree field of view and at varying incident angles the solid segments in Fig. 3 clearly show further improvements. The applied corrections vary from 13.4 cm for a straight view to 19.4 cm for a view at maximum angle.

### 4.2 Visibility Deviation

The error due to misalignment angle corrupts visibility tree; first at the edges of initial transmission regions, i.e., depth 1 transmission branches, and consequently the shapes of deeper reflection and transmission regions. The corrupt visibility tree erroneously proclaims some areas being visible and others being hidden, which affects signal accumulation in the backtracking step. It has to be noted here that the double refraction misalignment error affects only visibility of objects while the through-wall path of a viable ray still remains precise. Namely, once a location of a receiver is confirmed to be visible, signal is accumulated by retracing the exact propagation path down to the source. The signal accumulation procedure can be any standard technique of summing coherent rays taking into account antenna pattern, polarization, material composition, frequency, etc.

In order to evaluate the extent of visibility tree corruption in a real scenario, we designed a series of tests in which a visibility count is maintained by each

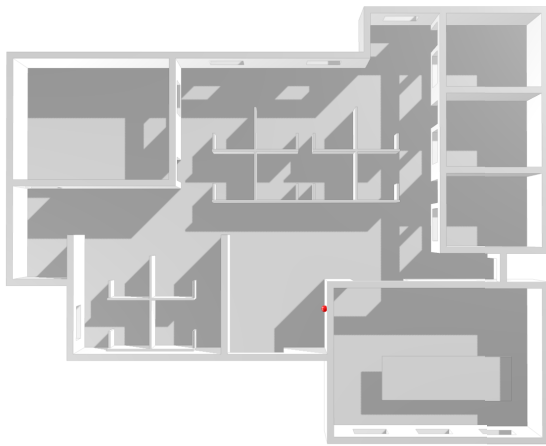


Fig. 4. Office test scenario with transparent ceiling

reception point, effectively summing up the number of reflected and double-refracted wavefronts hitting a reception point.

Two wireless planning tools were employed. The method of image was implemented as an indoor wireless planner tool. As the reference not affected by the misalignment type of error, in-house tool based on the shooting and bouncing rays (SBR) was used. The SBR tool has been already proven in several projects with telecommunication industry. It is highly optimized GPU-based ray tracer using the NVIDIA OptiX ray-tracing engine, which is adapted to the radio propagation environment. The reference tool was selected over other commercially available prediction tools because it could be fully customized. Diffraction and scattering have been disabled as these effects are not supported by the imaging technique. Knowing all the intricate details of the implementation, no shortcuts, such as dividing surfaces into tiles and other closely-guarded trade secrets of commercial tools, could bias the comparison.

The following results refer to the office scenario shown in Fig. 4. The prediction plane is located at 1.1 m above the ground with 30 reception points per meter. The transmitting dipole operates at Wi-Fi frequency of 2.5 GHz. It is positioned near the office entrance at 2.2 m above the ground and at 45-degree inclination (red dot).

Fig. 5 shows the difference in wavefront count between the uncorrected MI and the SBR for rays encountering single reflection/transmission. In image tree terminology, we are observing visibility error at tree depth 1. Visibility difference shows as beam-shaped areas originating in the corners, either being erroneously visible (+1) or being erroneously hidden (-1). The effect is most prominent for walls close to the transmission point. On the other hand, applying

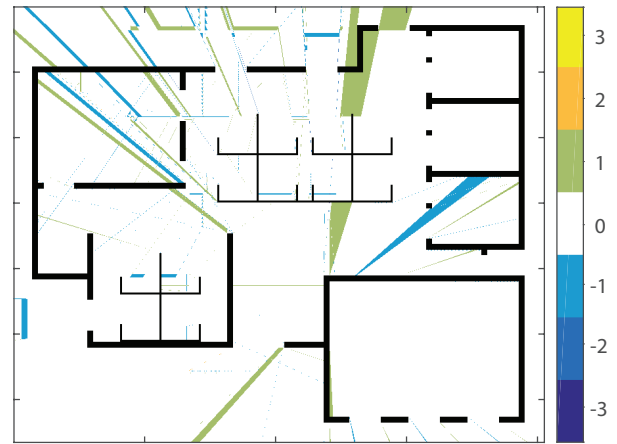


Fig. 5. Wavefront count difference between reference SBR and uncorrected MI at image tree depth 1



Fig. 6. Wavefront count difference between reference SBR and source-translated MI at image tree depth 1

correction  $\Delta$  reduces the most severe deviations, as evident in Fig. 6.

First it may seem that the improvement is relatively small and the misalignment may well be ignored. However, the visibility error spreads into deeper reflections/transmissions regions. In Fig. 7, the visibility incorrect areas extend over large portion of reception points at tree depth 2, with some reception points missing or being struck by multiple erroneous wavefronts. The problem is considerably reduced with the proposed source image translation as shown in Fig. 8.

Wavefront analysis for ray paths with number of interactions above 2 is less informative because wavefront count fails to record the difference in signal strength of ray paths hitting the same reception point. Thus, in Fig. 9 we compare actual signal loss computed by the SBR and the uncorrected MI for ray paths involving up to 4 interactions.

Difference of the two predictions has zero mean

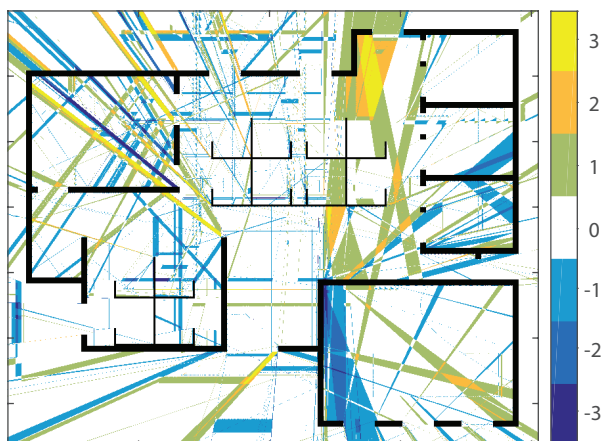


Fig. 7. Wavefront count difference between reference SBR and uncorrected MI at image tree depth 2

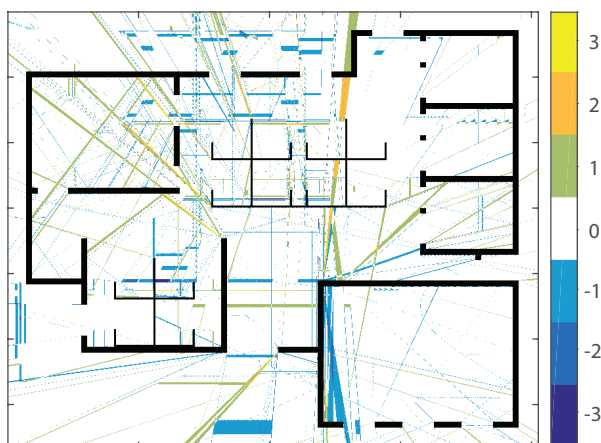


Fig. 8. Wavefront count difference between reference SBR and  $\Delta$ -corrected MI at image tree depth 2

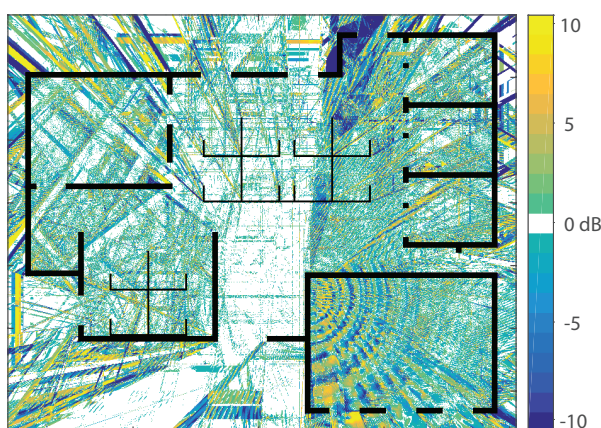


Fig. 9. Difference in predicted signal loss between reference SBR and uncorrected MI for ray paths with up to 4 scene interactions

and standard deviation less than 4.5 dB for 99% of reception points. When applied to the difference be-

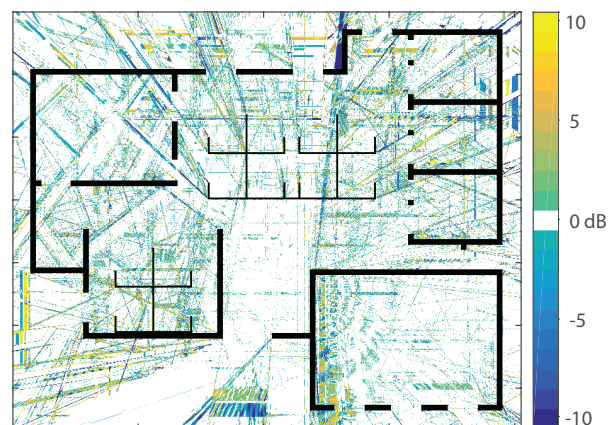


Fig. 10. Difference in predicted signal loss between reference SBR and  $\Delta$ -corrected MI for ray paths with up to 4 scene interactions

tween the reference SBR and  $\Delta$ -corrected MI, standard deviation as defined above drops to 2.4 dB. Further, in Fig. 10 significantly less area is affected by the misalignment error. Signal field is much smaller after several through-wall transmissions in the studied scenario; hence further increasing the number of interactions had less influence on the prediction difference.

Although the SBR implementation served as a reference, it has to be noted that some error should be attributed to the use of reception spheres in the SBR alone. In the above tests, disproportionately small reception spheres with 3 mm radius have been used in order to minimize that type of error. Consequently, 2G rays have been launched per test with running times of up to 2 hours to guarantee at least one hit for rays experiencing maximum number of interactions. On the other hand, MI execution times have been typically under a minute.

## 5 Conclusion

This paper studies the distortion of a bounding volume due to a double refraction on parallel planes. The distortion influences the accuracy of the method of images if strict visibility tree is used for signal prediction. The misalignment error is proposed to be minimized by the source image translation, which makes strict visibility trees a viable method of choice even if through-wall transmission needs to be modeled.

**Acknowledgement:** The research was supported by the Slovenian Research Agency (Grant No. L2-7664).

*References:*

- [1] M. Kimpe, H. Leib, O. Maquelin and T.H. Szymanski, Fast Computational Techniques for Indoor Radio Channel Estimation, *Comput. Sci. Eng.*, Vol. 1, No. 1, 1999, pp. 31–41.
- [2] Z. Yun and M. Iskander, Ray Tracing for Radio Propagation Modeling: Principles and Applications, *IEEE Access*, Vol. 3, 2015, pp. 1089–1100
- [3] F. Ikegami, T. Takeuchi, and S. Yoshida, Theoretical Prediction of Mean Field Strength for Urban Mobile Radio, *IEEE Trans. Antennas Propag.*, Vol. 39, No. 3, 1991, pp. 299–302.
- [4] D.A. McNamara, C.W.I. Pistorius, and J.A.G. Malherbe, *Introduction to the Uniform Geometrical Theory of Diffraction*, Antennas and Propagation Library, Artech House, Norwood, MA, 1990.
- [5] J. Stam, Diffraction Shaders, *Proceedings of the 26th Annual Conference on Computer Graphics and Interactive Techniques (SIGGRAPH)*, Los Angeles, CA, 1999, pp. 101–110.
- [6] S. Fortune, A Beam-Tracing Algorithm for Prediction of Indoor Radio Propagation, *Selected Papers from the Workshop on Applied Computational Geometry, Towards Geometric Engineering*, 1996, pp. 157–166.
- [7] J. Maurer, O. Drumm, D. Didascalou and W. Wiesbeck, A Novel Approach in the Determination of Visible Surfaces in 3D Vector Geometries for Ray-Optical Wave Propagation Modelling, *Proceedings of the 51st IEEE Vehicular Technology Conference (VTC 2000-Spring)*, Tokyo, Japan, Vol. 3, 2000, pp. 1651–1655.
- [8] F. Agelet, A. Formella, J. Hernando Rabanos, F. de Vicente and F. Fontan, Efficient Ray-Tracing Acceleration Techniques for Radio Propagation Modeling, *IEEE Trans. Veh. Technol.*, Vol. 49, No. 6, 2000, pp. 2089–2104.
- [9] R. Novak, Discrete Method of Images for 3D Radio Propagation Modeling, *3D Research*, Vol. 7, No. 3, 2016, pp. 26:1-26:12.
- [10] T. Rautiainen, R. Hoppe and G. Wolffe, Measurement and 3D Ray Tracing Propagation Predictions of Channel Characteristics in Indoor Environments, *IEEE 18th International Symposium on Personal, Indoor and Mobile Radio Communications (PIMRC)*, Athens, Greece, 2007, pp. 1–5.
- [11] M. Ashour, S. Micheal, A. Khaled, T. el Shabrawy and H. Hammad, A Pre-processing Dependent Image Theory Based Ray Tracing Algorithm for Indoor Coverage Solution, *Proceedings of the Wireless Communications and Networking Conference (WCNC)*, Istanbul, Turkey, 2014, pp. 299–304.
- [12] T.E. Athanaileas, G.E. Athanasiadou, G.V. Tsoulos and D.I. Kaklamani, Parallel Radio-Wave Propagation Modeling with Image-Based Ray Tracing Techniques, *Parallel Comput.*, Vol. 36, No. 12, 2010, pp. 679–695.
- [13] C. Rappaport, A Novel, Non-Iterative, Analytic Method to Find the Surface Refraction Point for Air-Coupled Ground Penetrating Radar, *Proceedings of the 5th European Conference on Antennas and Propagation (EUCAP)*, Rome, Italy, 2011, pp. 1786–1789.